Electronic supplementary information (ESI)

A carbon nanomaterial derived from nanoscale covalent organic framework for photothermal therapy in the NIR–II biowindow

Qun Guan, Le-Le Zhou, Li-Na Zhou, Mengdi Li, Guo-Xin Qin, Wen-Yan Li, Yan-An Li,* Yu-Bin Dong*

College of Chemistry, Chemical Engineering and Materials Science, Collaborative Innovation Center of Functionalized Probes for Chemical Imaging in Universities of Shandong, Key Laboratory of Molecular and Nano Probes, Ministry of Education, Shandong Normal University, Jinan 250014, P. R. China.

* E-mail: yananli@sdnu.edu.cn (Y. -A. Li); yubindong@sdnu.edu.cn (Y. -B. Dong).

1. Materials and instrumentation

1,3,5-Tris(4-aminophenyl)benzene (TPB) and 2,5-dimethoxyterephthaldehyde (DMTP) were purchased from Jilin Chinese Academy of Sciences - Yanshen Technology Co., Ltd. Benzaldehyde and polyvinyl pyrrolidone (PVP, Mw = 8000) were purchased from Aladdin Reagent Co., Ltd. All organic solvents were purchased from Sinopharm Chemical Reagent Co., Ltd. All reactants were used as purchased without further purification. Ultra-pure water was prepared with an Aquapro System (18 MΩ).

Hoechst 33258, calcein acetoxymethyl ester (calcein-AM), propidium iodide (PI), 2',7'-dichlorodihydrofluorescein diacetate (DCFH-DA), acridine orange (AO), and Cy5 (CAS# 146368-11-8) were purchased from MedChemExpress Co. Ltd. Fluorescein-5-isothiocyanate (FITC) and doxorubicin hydrochloride (DOX) were purchased from TCI (Shanghai) Development Co., Ltd. Cell Counting Kit 8 (CCK-8) was purchased from Dojindo (Shanghai, P. R. China). Phalloidin-iFluor 633 was purchased from Abcam (Shanghai, P. R. China). Paraformaldehyde fix solution was purchased from Biosharp (Hefei, P. R. China). Human serum albumin (HSA) was purchased from Beijing Solarbio Science & Technology Co., Ltd.

Phosphate-Buffered Saline (PBS), Dulbecco's Phosphate-Buffered Saline (DPBS), and Fetal Bovine Serum (FBS) were purchased from Biological Industries USA, Inc. Hank's Balanced Salt Solution (HBSS) was purchased from Gibco (Thermo Fisher Scientific). Dulbecco's Modified Eagle Medium (DMEM), Roswell Park Memorial Institute 1640 Medium (RPMI-1640), Penicillin Streptomycin Mixtures (Pen-Strep), and Trypsin-EDTA Solution (0.25%) were purchased from HyClone Laboratories, Inc. Normocin was purchased from Invivogen (San Diego, CA, USA).

Fourier transform infrared (FT-IR) spectra were obtained in the 4000–400 cm^{-1} range using a Thermo Scientific Nicolet iS50 FT-IR Spectrometer equipped with a diamond attenuated total reflection (ATR) module. Each spectrum was the average of 16 scans. Ultraviolet–visible–near-infrared (UV–vis–NIR) absorption spectra were recorded on a Shimadzu UV-2600 Double Beam UV−vis Spectrophotometer. Transmission electron microscopy (TEM) images were recorded on a Hitachi HT7700 120 kV Compact-Digital Transmission Electron Microscope. High-resolution transmission electron microscopy (HRTEM) images were recorded on a JEOL 2100 200 kV Transmission Electron Microscope equipped with an Energy Dispersive X-ray Spectrometer (EDS). Scanning electron microscopy (SEM) images were recorded on a Hitachi SU8010 Scanning Electron Microscope. Raman spectra were collected on a HORIBA LabRAM HR Evolution Raman Microscope using 532 nm excitation wavelength. X-ray photoelectron spectroscopy (XPS) profiles were obtained on a Thermo Fisher Scientific ESCALAB 250Xi XPS System equipped with a monochromatic Al Kα radiation source (1486.6 eV). Elemental microanalyses (EA) were performed using an Elementar Vario EL Cube Elemental Analyzer. TGA curves were obtained on a Mettler Toledo TGA/DSC3+ Thermogravimetric Analyzer with high temperature furnace (HT). Powder X-ray diffraction (PXRD) patterns were obtained on a Rigaku SmartLab SE X-Ray Powder Diffractometer with Cu Kα line focused radiation (λ = 1.5405 Å) from 2θ = 2.00° up to 90.00° with 0.01° increment. Nitrogen-adsorption isotherms were measured at 77 K with a Micromeritics ASAP2020 HD88 Surface Area and Porosity Analyser. Before measurement, the samples were degassed in vacuum at 120 °C for 12 h. The Brunauer–Emmett–Teller (BET) equation was used to calculate the specific surface areas. The pore size distribution was derived from the sorption curve using the non-local density functional theory (NLDFT) model. Hydrodynamic particle size and Zata potential were measured using Malvern Zetasizer Nano ZS90 System. Laser scanning confocal fluorescence images were captured with a Leica TCS SP8 Confocal Laser Scanning Microscopy, using glass bottom dishes purchased from Cellvis (Mountain View, CA, USA). Microplate assays were carried out on a Molecular Devices SpectraMax i3x Multi-Mode Microplate Detection System. *In vivo* and *ex vivo* fluorescence images of mice

were captured with a PerkinElmer IVIS Spectrum *In Vivo* Imaging System.

2. Cell culture and experimental animals

MCF-7 (human breast adenocarcinoma) and Jurkat (acute T cell leukemia) cell lines were provided by Institute of Basic Medicine, Shandong Academy of Medical Sciences (Jinan, P. R. China). The MCF-7 cells were cultured in DMEM supplemented with FBS (10 vol%), Normocin (100 μg/mL), penicillin (100 U/mL), and streptomycin (100 μg/mL) in a 5% CO_2 atmosphere at 37°C. The Jurkat cells were cultured in RPMI-1640 supplemented with FBS (10 vol%), Normocin (100 μg/mL), penicillin (100 U/mL), and streptomycin (100 μg/mL) in a 5% CO_2 atmosphere at 37°C.

Animal experiments were reviewed and approved by the Ethics Committee of Shandong Normal University (Jinan, P. R. China). All the animal experiments complied with relevant guidelines of the Chinese government and regulations for the care and use of experimental animals. Nude mice (BALB/cJGpt-*Foxn1*^{nu}/Gpt, aged 4 weeks) were purchased from GemPharmatech (Nanjing, P. R. China). The nude mice were housed in a pathogen-free facility and kept in a temperature-controlled room set to a light and dark cycle of 12 h each. To establish the MCF-7 xenograft model, MCF-7 cancer cells (~10^6 cells) suspended in HBSS (50 μL) were subcutaneously injected into the flanks of each mouse. Length (L) and width (W) of the tumor were determined using digital calipers. The tumor volume (*V*) was calculated by the formula: $V = 1/2 \times L \times W^2$.

3. Synthesis and characterizations of TD-COF

After the mixture of TPB (984 mg, 2.8 mmol), DMTP (816 mg, 4.2 mmol), and polyvinyl pyrrolidone (1000 mg) in acetonitrile (1000 mL), acetic acid (50 mL) was added, the mixture was stirred at 25°C for 24 h. Then, benzaldehyde (400 μL, 4.0 mmol) was added to the mixture to terminate the reaction. After 1 h, the generated TD-COF nanoparticles were isolated by centrifugation and washed thoroughly with acetonitrile and ethanol. After being dried at 80°C for 12 h, TD-COF was obtained as a yellow crystalline powder.

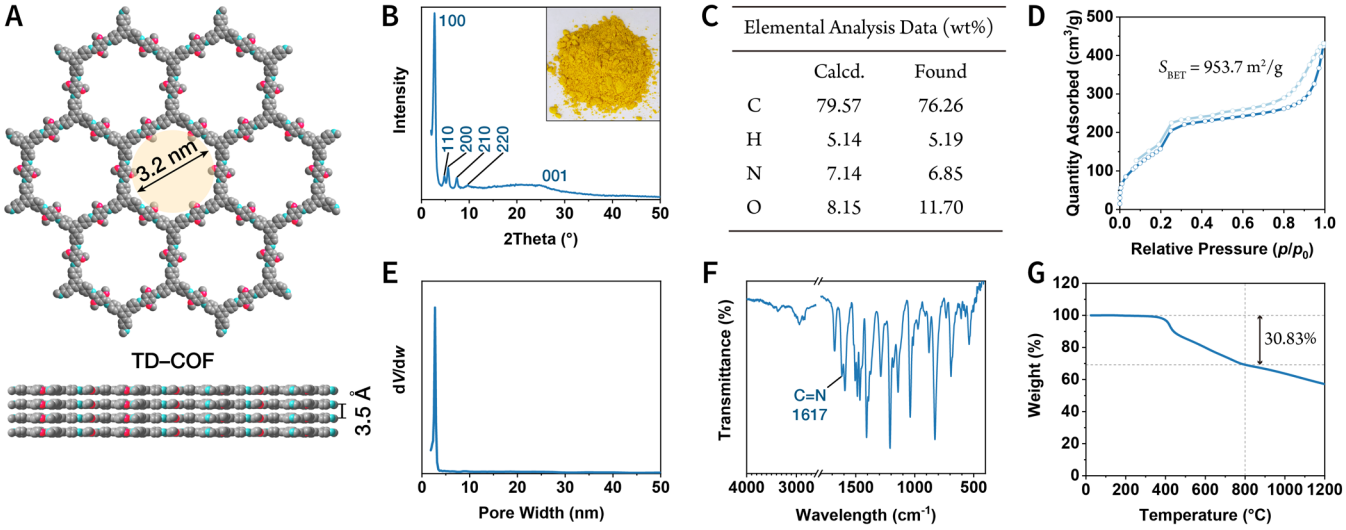

Fig. S1 Characterizations of TD-COF. (A) The packing models of TD-COF indicating the pore aperture and π-π stacking distances. (B) PXRD pattern of TD-COF. Inset: Digital photo of TD-COF powder. (C) Elemental analysis data of TD-COF ($C_{78}H_{60}N_6O_6$). (D) N_2 adsorption and desorption isotherms of TD-COF at 77 K. (E) Pore width distribution plot of TD-COF. (F) FT-IR spectrum of TD-COF. (G) TGA curve of TD-COF.

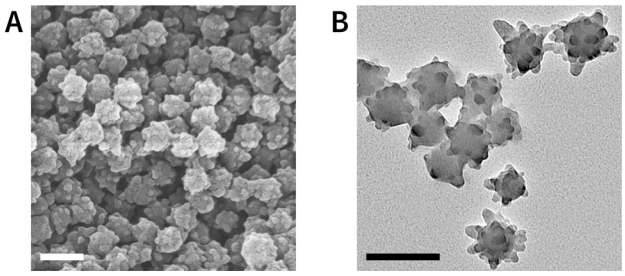

Fig. S2 (A) SEM image of TD-COF. Scale bar, 200 nm. (B) TEM image of TD-COF. Scale bar, 200 nm.

4. Synthesis of CNP

TD-COF (500 mg) was carbonized at 800°C for 2 h under an Ar atmosphere flow in a tube furnace at a heating rate of 5°C/min. CNP was obtained as a black powder. Yield: 340 mg.

5. BET analysis of CNP

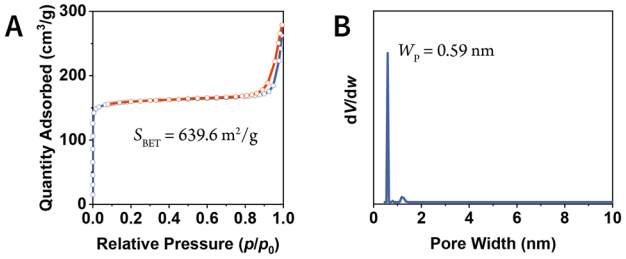

Fig. S3 (A) N_2 adsorption and desorption isotherms at 77 K of CNP. (B) Pore width distribution plot of CNP.

6. XPS spectra of CNP

The XPS spectra of CNP showed three main peaks at the binding energy of 284.6, 400.6 and 532.6 eV, corresponding to C1s, N1s and O1s, respectively (Fig. S4A).

The high-resolution XPS C1s spectra of CNP can be deconvoluted into five peaks, C-C and C=C at 284.8 eV, C=N at 286.1 eV, C-O at 287.0 eV, C=O at 288.0 eV, and π-π* satellite at 290.1 eV (Fig. S4B). Similarly, the peak-fitted high-resolution spectra of N1s correspond to the pyridinic N at 398.4 eV, pyrrolic N at 399.4 eV, graphitic N at 400.9 eV, and oxidized N at 403.4 eV (Fig. S4C). Meanwhile, the O1s spectra can be differentiated and fitted into two peaks, C-O at 531.6 eV and C=O at 533.5 eV (Fig. S4D).[1]

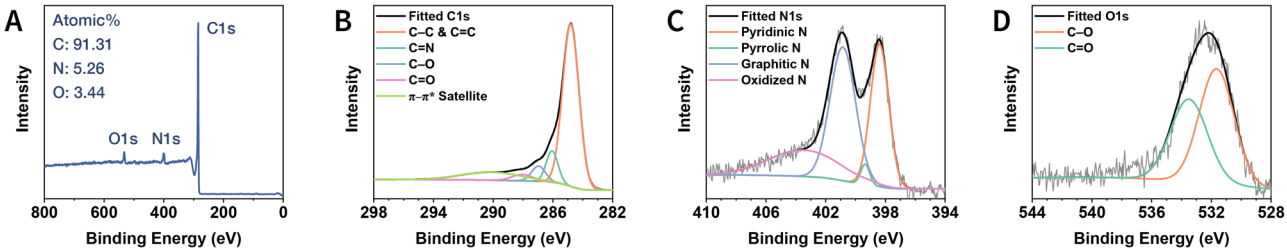

Fig. S4 (A) XPS survey scan spectrum of CNP. (B–D) High-resolution (B) C1s, (C) N1s, and (D) O1s XPS narrow scan spectra.

7. High-resolution TEM images of CNP

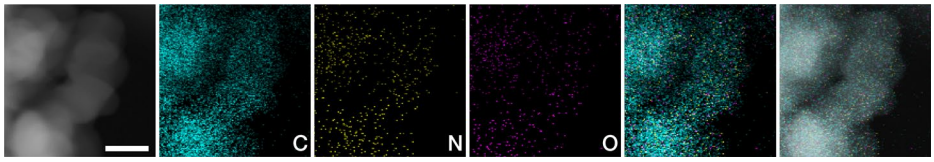

Fig. S5 HRTEM and elemental mapping images. Scale bar, 100 nm. The element distributions well match with the globular appearance observable in the HRTEM images.

8. DLS measurements of CNP

As indicated in Fig. S6, CNP had an average hydrodynamic diameter (Z-average size) of 108.0 nm and a polydispersity index (PDI) of 0.112, suggesting that CNP was basically monodisperse in PBS. When the CNP suspension in PBS was allowed to sit at room temperature for 6 and 12 h, no significant changes in Z-average size and PDI were observed. After 24 h, still no megascopic particulate matter appeared, but its Z-average size and PDI increased to 281.9 nm and 0.520, respectively; indicating that the aggregation of the CNP occurred to some extent. This phenomenon is consistent with the previous observation on the naked carbon-based particles.[2-4] So, the CNP suspension in PBS could be for stable at least 12 h under ambient conditions, which fully met the requirement of antitumor treatment *via* PTT. Similar trends were observed in DMEM and RPMI-1640 medium (Fig. S7).

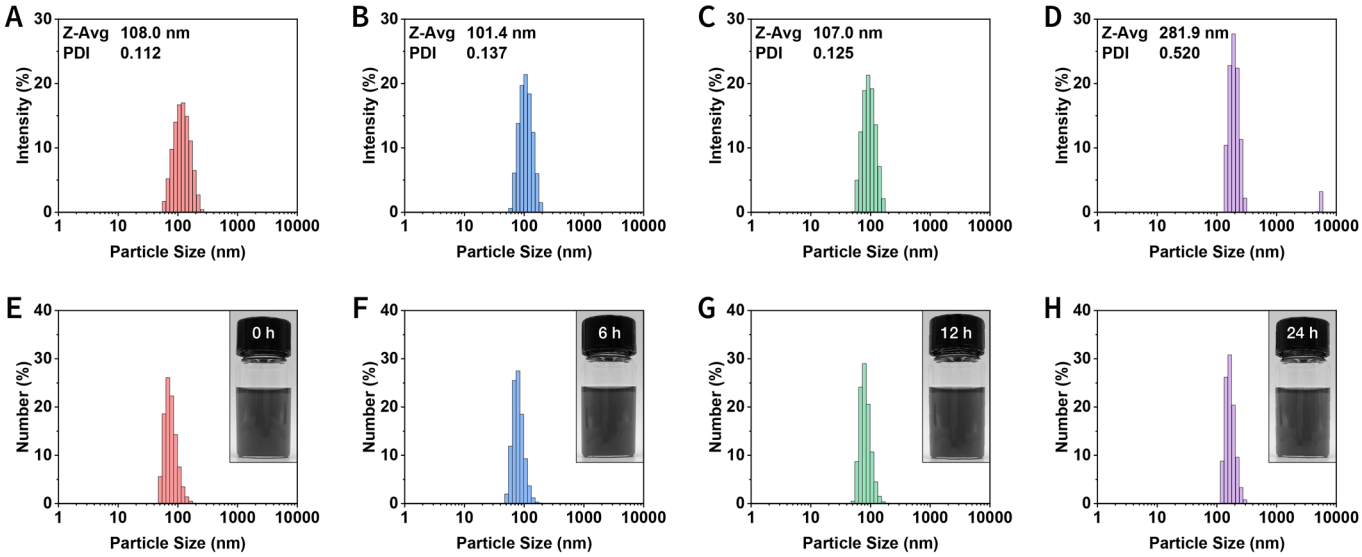

Fig. S6 Dynamic light scattering (DLS) of CNP/PBS suspension (800 μg/mL) at (A, E) 0 h, (B, F) 6 h, (C, G) 12 h, and (D, H) 24 h. The results were expressed in (A–D) intensity and (E–H) number, respectively. Inset: Digital photo of CNP suspension.

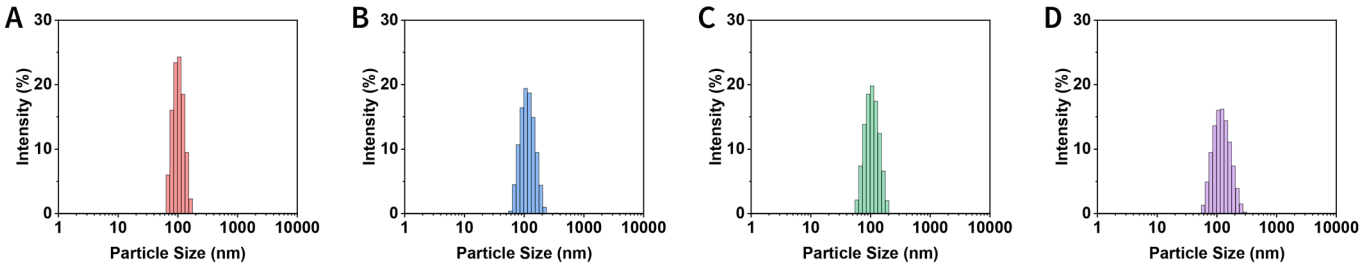

Fig. S7 DLS of CNP suspension in (A, B) DMEM and (C, D) RPMI-1640 at (A, C) 0 h and (B, D) 12 h.

9. Protein corona of CNP

To evaluate the CNP-protein interaction, human serum albumin (HSA), the main protein in human plasma, was selected as a model protein. As shown in Fig. S8, after stirring for 12 h, the amount of HSA adsorbed on the CNP surface is less than 10% of its own weight. Since the molecular size of HSA (4×4×12 nm) is larger than the pore size of CNP (0.59 nm), the possibility of host-guest encapsulation is excluded. And the zeta potential measurement shows that CNP has a negative surface charge (-11.3±0.8 mV), which may be the reason for the weak interaction between CNP and electronegative HSA (pI = 4.7).

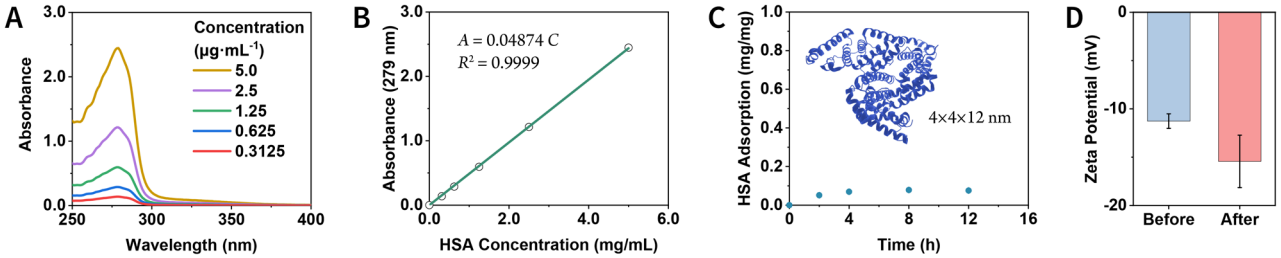

Fig. S8 (A) UV–vis absorption spectra of HSA solution. (B) Standard curve of HSA. (C) Quantitative research of HSA adsorption on the surface of CNP. (D) Zeta potentials of CNP before and after adsorbing HSA. Data were presented as mean ± SD (n = 4).

Experimentally, the CNP suspension (1.0 mL, 2.0 mg/mL) were mixed with HSA solution (1.0 mL, 5.0 mg/mL). After stirring for different, the dispersion was centrifuged, and the supernatant was taken for protein concentration detection based on standard curve method.

10. Photothermal conversion efficiency

The CNP suspension (1.0 mL, 800 μg/mL) was added in a quartz dish and irradiated with a 1064 nm laser (1.0 W/cm^2) for 10 min. Then, the laser was turned off to allow the suspension to cool naturally. The temperature of the dispersion was recorded at 10 s intervals. The photothermal conversion efficiency[5] was calculated according to the following formulas:

$$\eta = \frac{Q_{\mathrm{s}} - Q_{\mathrm{w}}}{I(1 - 10^{-A_{1064}})} \quad ;$$

$$hS = \frac{mc}{\tau} \quad ;$$

$$Q_{\mathrm{s}} = hS\Delta T_{\mathrm{s,h}} \quad ;$$

$$\tau = -\frac{\mathrm{d}t}{\mathrm{d}\ln\theta} \quad ;$$

$$Q_{\mathrm{w}} = hS\Delta T_{\mathrm{w,h}} \quad ;$$

$$\theta = \frac{T_{t,c} - T_{\mathrm{min,c}}}{\Delta T_{\mathrm{s,c}}} \quad .$$

Where η represented photothermal conversion efficiency; A_{1064} represented the absorption of solution at 1064 nm; I represented the power of the laser; $\Delta T_{\mathrm{s,h}}$ represented the changed temperature of solution in the heating curve; $\Delta T_{\mathrm{w,h}}$ represented the changed temperature of water in the heating curve; c represented specific heat capacity of water; m represented solution mass; τ represented the slope of $t-(-\ln\theta)$ graph; t represented time in the cooling curves; $\Delta T_{\mathrm{s,c}}$

represented the changed temperature of solution in the cooling curve; $T_{\min,c}$ represented the final temperature of solution in the cooling curve; and $T_{t,c}$ represented the temperature of solution at different times in the cooling curve.

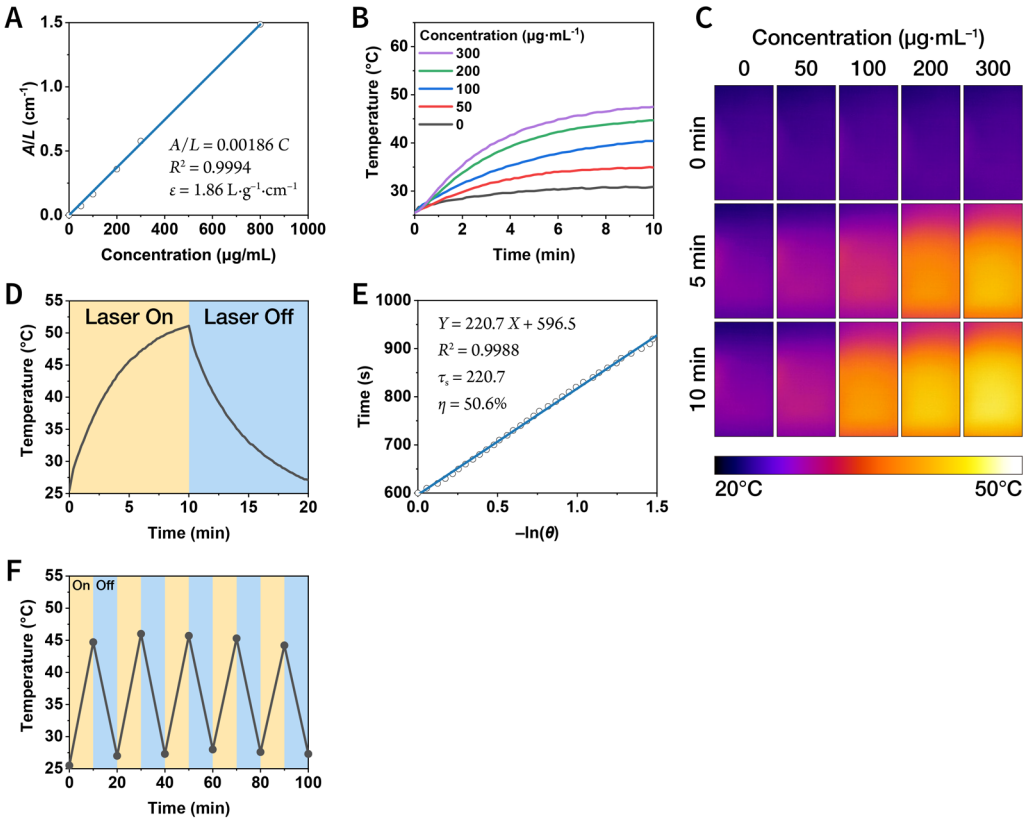

Fig. S9 (A) Mass extinction coefficient (ε) of CNP suspension at 1064 nm. A/L: Absorbance at λ = 1064 nm divided by the optical path length of the cuvette. (B) Photothermal heating curves of CNP suspensions with different concentrations under irradiation of a 1064 nm laser (1.0 W/cm^2). (C) Thermal images of CNP suspensions with different concentrations under the irradiation of a 1064 nm laser (1.0 W/cm^2). (D) Photothermal effect of CNP suspension (800 μg/mL) under the irradiation of a 1064 nm laser (1.0 W/cm^2) for 10 min, and then the laser was switched off to allow natural cooling. (E) Time constant (τ_s) calculated from the cooling period after the laser was turned off. (F) Recycling heating curves of CNP suspension (200 μg/mL) under irradiation of a 1064 nm laser (1.0 W/cm^2).

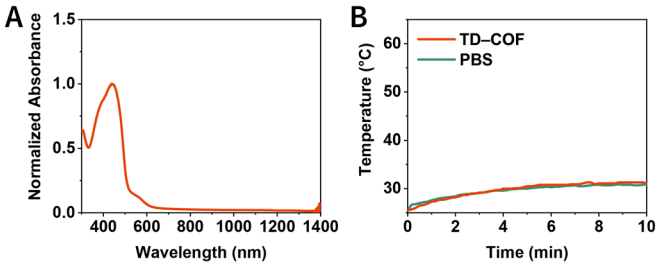

Fig. S10 (A) UV–vis–NIR absorption spectrum of TD-COF suspension. (B) Photothermal heating curves of PBS and TD-COF suspension (200 μg/mL) under irradiation of a 1064 nm laser (1.0 W/cm^2).

11. CCK-8 assays to evaluate cytotoxicity *in vitro*

To assess the effect of CNP concentration on PTT, a concentration-dependent CCK-8 assay was performed. In brief, cells were seeded into 96-well plates with a cell number of ~5k cells/well and incubated overnight in a CO_2 incubator. After removal of the

culture medium, the cells were incubated with CNP suspension (100 μL, 0–300 μg/mL) for 2 h in a CO_2 incubator, and then exposed to a 1064 nm laser (0 or 1.0 W/cm^2) for 10 min. After additional 24 h incubation, the cell viability was measured using a CCK-8 assay. The cells without treatment were used as the control.

12. Calcein-AM/PI double staining

Cells were seeded into glass bottom dishes and incubated overnight in a CO_2 incubator. After removal of the culture medium, the cells were incubated with CNP suspension (100 μL, 0 or 300 μg/mL) for 2 h in a CO_2 incubator, and then exposed to a 1064 nm laser (0 or 1.0 W/cm^2) for 10 min. After an additional 4 h incubation, the cells were co-incubated with calcein-AM (500 μL, 2 μM) and PI (500 μL, 4 μM) for 15 min, and the laser scanning confocal fluorescence images were captured. The green images of living cells were excited by a 488 nm light, and the emission wavelength range was collected at 520±20 nm. The red images of dead cells were excited by 514 nm light, and the emission wavelength range was collected at 640±20 nm. The results were shown in Fig. S11.

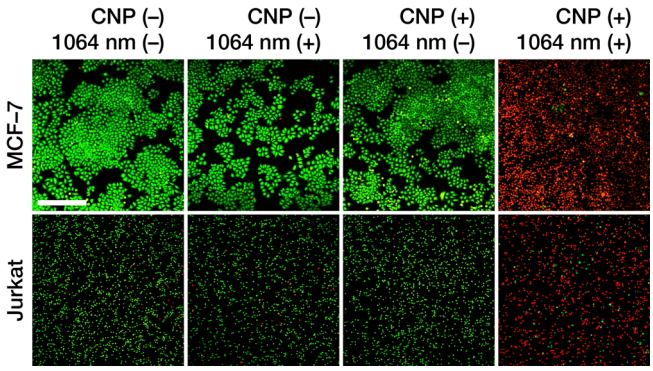

Fig. S11 Calcein-AM/PI double staining experiments. The cells that were pre-incubated with CNP dispersion (0 or 300 μg/mL, 2 h) were exposed to a 1064 nm laser (1.0 W/cm^2, 0 or 10 min). After an additional 4 h incubation, the cells were co-stained with calcein-AM (green, living cells) and PI (red, dead cells), and imaged using confocal laser scanning microscopy. Scale bar, 500 μm.

13. Internalization of CNP in tumor cells

To confirm the internalization of CNP in tumor cells, CNP was loaded with PI, a cell membrane impermeable cationic dye. The obtained PI@CNP was incubated with MCF-7 cells, and then the nuclei were labeled using a membrane permeable fluorescent dye Hoechst 33258. As revealed in Fig. S12, confocal laser scanning microscopical images showed that PI cannot penetrate the membrane of living cells, but can cross the cell membrane of fixed cells and localize to the nucleus. In sharp contrast, PI@CNP can penetrate the cell membrane of living cells and form spot-like fluorescence in the cytoplasm, suggesting that CNP changed the subcellular localization of PI, thus proving that PI enters living cells by virtue of CNP carriers. In order to provide further evidences of cellular internalization, on the basis of the method suggested in the reference,[6-10] three other fluorescent dyes, FITC (an anionic dye), DOX (a neutral drug molecule) and Cy5 (a dye with broad conjugated system), were also loaded into CNP. As shown in Fig. S13, obviously, the intracellular spot fluorescence induced by FITC@CNP, DOX@CNP, and Cy5@CNP was available. Taken together, these interesting results showed that CNP can effectively penetrate living cells and localize in the cytoplasm.

Experimentally, X@CNP (X = PI, FITC, DOX, Cy5) was prepared as follows: first, X (1 mg), CNP (1 mg) was added to DMSO (1.0 mL); then, the suspension was stirred for 24 h in the dark; next, the supernatant was discarded after centrifugation, and the solids were fully washed with PBS; finally, the solid was re-dispersed into PBS (1.0 mL) to obtain stock solution of X@CNP (1.0 mg/mL, CNP equiv.). For cell experiment, MCF-7 cells were seeded into glass bottom dishes and incubated overnight in a CO_2 incubator. After removal of the culture medium, the cells were incubated using X@CNP suspension (1.0 mL, 100 μg/mL, CNP equiv.) for 2 h in a CO_2 incubator, and washed with DPBS twice. Finally, the laser scanning confocal fluorescence images were captured. The images of PI were excited by 514 nm light, and the emission wavelength range was collected at 640±20 nm. The images of Hoechst 33258 were excited by 405 nm light, and the emission wavelength range was collected at 460±20 nm. The images of FITC were excited by 488 nm light, and the emission wavelength range was collected at 520±20 nm. The images of DOX were excited by 488 nm light, and the emission wavelength range was collected at 600±20 nm. The images of Cy5 were excited by 633 nm light, and the emission wavelength range was collected at 670±30 nm.

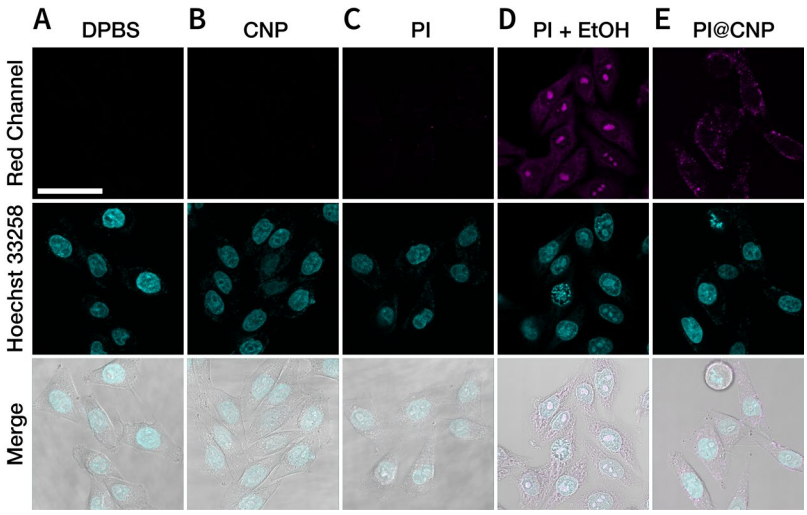

Fig. S12 Transmembrane transport of CNP using PI as fluorescent marker. (A) Untreated cells. (B) Cells incubated with CNP. (C) Cells incubated with PI. (D) Fixed cells incubated with PI. (E) Cells incubated with PI@CNP. Scale bar, 50 μm.

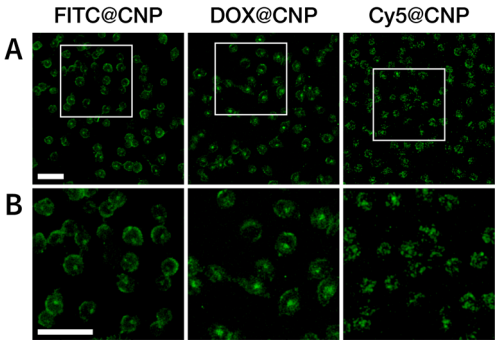

Fig. S13 Transmembrane transport of CNP using FITC, DOX, and Cy5 as fluorescent markers. Scale bar, 50 μm.

To assess the effect of cell uptake on PTT, an incubation time-dependent CCK-8 assay was performed (Fig. S14). In brief, MCF-7 cells were seeded into 96-well plates with a cell number of ~5k cells/well and incubated overnight in a CO_2 incubator. After removal of the culture medium, the cells were incubated with CNP suspension (100 μL, 50 or 200 μg/mL) for 0, 2, 6, and 12 h in a CO_2 incubator, and then washed with DPBS twice carefully. Next, the cells exposed to a 1064 nm laser (1.0 W/cm^2) for 10 min. After additional 24 h incubation, the cell viability was measured. The cells without any treatment were used as the control.

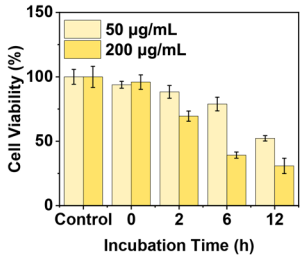

Fig. S14 Incubation time-dependent CCK-8 assay. The cells were incubated with CNP dispersion (50 or 200 μg/mL) for different time (0–12 h). After being carefully washed, the cells were exposed to a 1064 nm laser (1.0 W/cm^2, 10 min). Finally, after an additional 24 h incubation, the relative cell viabilities were detected using CCK-8 assays. Data were presented as mean ± SD (*n* = 3).

14. Cell death mechanism research

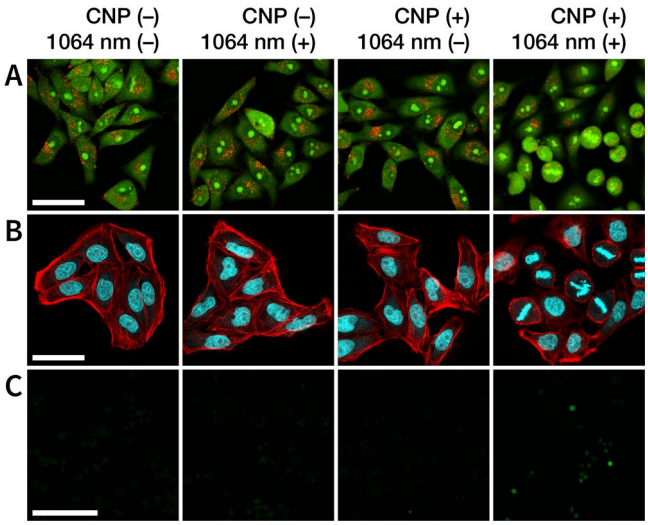

Fig. S15 PTT-induced subcellular effects studied with laser confocal imaging. (A) Detection of lysosomal membrane permeability using acridine orange. Scale bar, 50 μm. (B) Detection of cytoskeletal integrity using phalloidin-iFluor 633 (red). Nuclei were labeled using Hoechst 33258 (blue). Scale bar, 50 μm. (C) Detection of intracellular ROS using DCFH-DA (green). Scale bar, 250 μm. Experimentally, the cells pre-incubated with CNP (0 or 100 μg/mL, 2 h) were exposed to a 1064 nm laser (0 or 1.0 W/cm^2, 10 min). The confocal laser scanning microscopical images were acquired after staining using the fluorescent dye.

After the nanoparticles are taken up by the cells through pinocytosis, they usually enter the lysosome first.[11] The effect of CNP-induced PTT on lysosomes was assessed using acridine orange (AO) as fluorescent probe. AO emits red fluorescence in the lysosome of living cells due to protonation. When the permeability of the lysosomal membrane increases, AO leaks into the cytosol and deprotonates to emit green fluorescence. As illustrated in Fig. S15A, when MCF-7 cells were exposed to CNP or 1064 nm laser alone, red dot-like fluorescence was observed in the cells, which was no different from the control group. However, in cells undergoing PTT, red fluorescence was significantly reduced, and green fluorescence was enhanced, especially in cells that were rounded. These results confirmed that CNP-induced PTT significantly increased the lysosomal membrane permeability, which led to lysosomal damage.

Morphological changes such as cell rounding were observed in the above experiments. We speculated that the cytoskeleton, which is responsible for maintaining cell morphology, was damaged by the PTT-induced high temperature. The fibrous actin (F-actin) cytoskeleton, a dynamic structure necessary in regulating cell functions, was labeled using phalloidin-iFluor 633 fluorescent

staining, and the change in cytoskeleton organization of MCF-7 cells treated by CNP with and without 1064 nm laser irradiation were investigated. As shown in Fig. S15B, there was no obvious difference between the laser or CNP-treated cells and the untreated cells in the control group. In these three cell groups, F-actin proteins were legible and well organized in thick bundles of stress fibers. Thus, CNP had negligible influence on actin cytoskeleton organization and cell morphology. However, for the CNP and laser co-treated cells, F-actin was organized in a dispersive anisotropic network with rather sparsely formed filament bundles that accumulated in the cell. These results confirmed that CNP itself had good biocompatibility, but CNP-induced PTT could destroy the cytoskeletal integrity, consequently, led the cells from spindle to spherical shape.

High-temperature can cause cell oxidative stress and up-regulation of the intracellular reactive oxygen species (ROS).[12, 13] DCFH-DA staining showed that the CNP-induced high-temperature slightly increased the intracellular ROS upon being exposed to 1064 nm laser irradiation, which was particularly obvious in the cells with altered cell morphology (Fig. S15C). Thus, in addition to hyperthermia-induced cytotoxicity, PTT may also cause cell death through excessive ROS-induced oxidative damage. This tendency was also observed in gold nanorod (AuNR)-induced PTT.[14]

Experimentally, to evaluate lysosomal membrane permeabilization, cells were seeded into glass bottom dishes and incubated overnight in a CO_2 incubator. After removal of the culture medium, the cells were incubated using CNP suspension (1.0 mL, 0 or 100 μg/mL) for 2 h in a CO_2 incubator, and then exposed to a 1064 nm laser (0 or 1.0 W/cm^2) for 10 min. After an additional 4 h incubation, the cells were incubated with AO (200 μL, 15 μM) for 10 min, washed with DPBS twice, and the laser scanning confocal fluorescence images were captured. The green images were excited by a 488 nm light, and the emission wavelength range was collected at 530±20 nm. The red images were excited by a 488 nm light, and the emission wavelength range was collected at 640±20 nm. To evaluate cytoskeletal integrity, cells were seeded into glass bottom dishes and incubated overnight in a CO_2 incubator. After removal of the culture medium, the cells were incubated using CNP suspension (1.0 mL, 0 or 100 μg/mL) for 2 h in a CO_2 incubator, and then exposed to a 1064 nm laser (0 or 1.0 W/cm^2) for 10 min. After an additional 4 h incubation, the cells were fixed with formaldehyde fixation (1.0 mL). Then, the F-actin were labelled using phalloidin-iFluor 633 (200 μL, 1.0 μg/mL) for 90 min, and the nucleus were labeled with Hoechst 33258 (200 μL, 10 μM) for 30 min. Finally, the laser scanning confocal fluorescence images were captured. The blue images of the nucleus were excited by a 405 nm light, and the emission wavelength range was collected at 460±20 nm. The red images of phalloidin-iFluor 633 were excited by a 633 nm light, and the emission wavelength range was collected at 649±20 nm. To evaluate intracellular ROS level, cells were seeded into glass bottom dishes and incubated overnight in a CO_2 incubator. After the removal of the culture medium, the cells were incubated with CNP suspension (1.0 mL, 0 or 100 μg/mL) for 2 h in a CO_2 incubator, and then exposed to a 1064 nm laser (0 or 1.0 W/cm^2) for 10 min. After an additional 4 h incubation, the cells were incubated with DCFH-DA (200 μL, 100 nM) for 10 min, washed with DPBS twice, and the laser scanning confocal fluorescence images were captured. The green images were excited by a 488 nm light, and the emission wavelength range was collected at 525±20 nm.

15. *In vivo* and *ex vivo* fluorescence imaging

To evaluate the biodistribution of CNP, Cy5@CNP (200 μL, 800 μg/mL, CNP equiv.) was intratumorally injected. Then, MCF-7 tumor-bearing were anesthetized and imaged at different time using an *in vivo* imaging system with the excitation wavelength of 640 nm and emission wavelength of 680 nm. Then, the mice were killed to separate the organs and tumors for *ex vivo* imaging to determine the biodistribution pattern and retention in tumors of Cy5@CNP. The results were shown in Fig. S16.

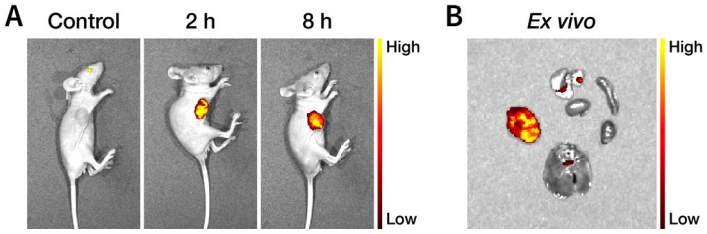

Fig. S16 *In vivo* and *ex vivo* imaging experiments. (A) Whole-body fluorescence images of MCF-7 tumor-bearing mice intratumorally injected with Cy5@CNP (200 μL, 800 μg/mL, CNP equiv.). (B) *Ex vivo* fluorescence imaging of each organ at 8 h.

16. Photothermal tumor eradication *in vivo*

When their tumor size reached ~100 mm^3, the nude mice bearing MCF-7 tumors (n = 20) were randomly distributed into four groups: (i) DPBS (3.0 mL/kg); (ii) CNP suspension (3.0 mL/kg, 800 μg/mL); (iii) DPBS (3.0 mL/kg), 1064 nm laser irradiation (1.0 W/cm^2, 10 min); (iv) CNP suspension (3.0 mL/kg, 800 μg/mL), 1064 nm laser irradiation (1.0 W/cm^2, 10 min). After intratumoral injection, for the group iii and iv, laser irradiation was performed on the tumor site. The nude mice continued to be fed for 14 days. The tumor volume and nude mouse body weight were recorded during the experimental period.

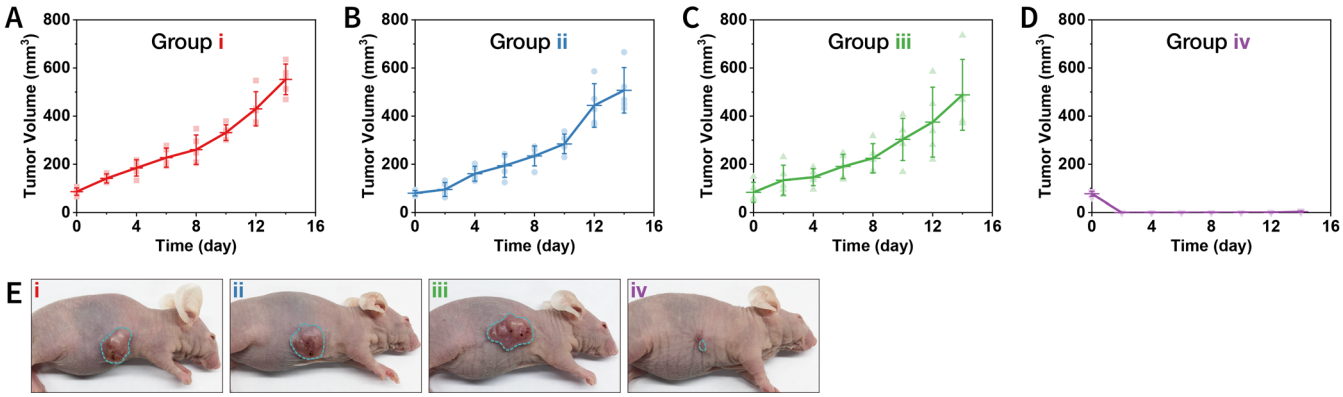

Fig. S17 (A–D) Tumor volume of each nude mice in various groups during the treatment. Data were presented as mean ± SD (n = 5). (E) Representative photographs of the nude mice at the end of the treatment.

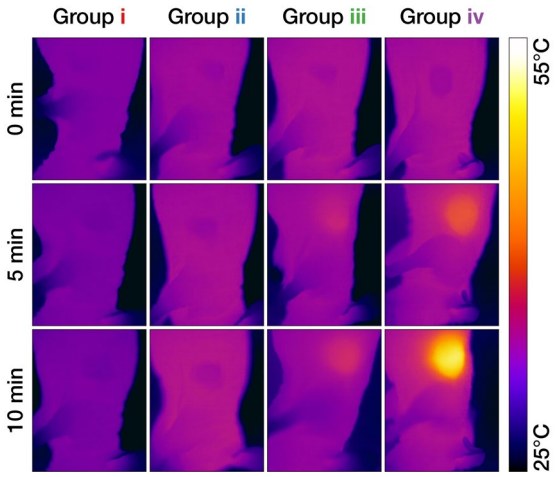

Fig. S18 Thermal imageries of the nude mice.

17. References

1. G. Greczynski and L. Hultman, *Prog. Mater Sci.*, 2020, **107**, 100591.
2. K. M. Isaac, I. V. Sabaraya, N. Ghousifam, D. Das, A. M. Pekkanen, D. K. Romanovicz, T. E. Long, N. B. Saleh and M. N. Rylander, *Carbon*, 2018, **138**, 309-318.
3. L. Wan, Q. Zhao, P. Zhao, B. He, T. Jiang, Q. Zhang and S. Wang, *Carbon*, 2014, **79**, 123-134.
4. Y. Yang, Y. Deng, J. Huang, X. Fan, C. Cheng, C. Nie, L. Ma, W. Zhao and C. Zhao, *Adv. Funct. Mater.*, 2019, **29**, 1900143.
5. H. Zhang, W. Zeng, C. Pan, L. Feng, M. Ou, X. Zeng, X. Liang, M. Wu, X. Ji and L. Mei, *Adv. Funct. Mater.*, 2019, **29**, 1903791.
6. M. Zhang, B. Xiao, H. Wang, M. K. Han, Z. Zhang, E. Viennois, C. Xu and D. Merlin, *Mol. Ther.*, 2016, **24**, 1783-1796.
7. H. Yin, X. Guan, H. Lin, Y. Pu, Y. Fang, W. Yue, B. Zhou, Q. Wang, Y. Chen and H. Xu, *Adv. Sci.*, 2020, **7**, 1901954.
8. C. Hu, Z. Zhang, S. Liu, X. Liu and M. Pang, *ACS Appl. Mater. Interfaces*, 2019, **11**, 23072-23082.
9. Y. Zhu, W. Lin, X. Wang, W. Zhang, L. Chen and Z. Xie, *Chem. Commun.*, 2018, **54**, 11921-11924.
10. Y. Zhang, J. Zhu, G. Huang, J. Zhu and D. He, *Carbon*, 2020, **163**, 128-136.
11. X. Cui, S. Xu, X. Wang and C. Chen, *Carbon*, 2018, **138**, 436-450.
12. D. M. Katschinski, K. Boos, S. G. Schindler and J. Fandrey, *J. Biol. Chem.*, 2000, **275**, 21094-21098.
13. R. Moniruzzaman, M. U. Rehman, Q.-L. Zhao, P. Jawaid, Y. Mitsuhashi, K. Sakurai, W. Heshiki, R. Ogawa, K. Tomihara, J.-i. Saitoh, K. Noguchi, T. Kondo and M. Noguchi, *Cancer Lett.*, 2019, **451**, 58-67.
14. M. Aioub, S. R. Panikkanvalappil and M. A. El-Sayed, *ACS Nano*, 2017, **11**, 579-586.

18. Author Contributions

Conceptualization, Q. Guan and Y.-B. Dong; Methodology, Q. Guan, Y.-A. Li, and Y.-B. Dong; Investigation, Q. Guan, L.-L. Zhou, L.-N. Zhou, M. Li, G.-X. Qin, W.-Y. Li, and Y.-A. Li; Writing – Original Draft, Q. Guan; Writing – Review & Editing, Q. Guan and Y.-B. Dong; Funding Acquisition, Y.-B. Dong and Y.-A. Li; Project Administration, Y.-B. Dong; Supervision, Y.-B. Dong.